Bismark C. Torrico
Department of Electrical Engineering,
Federal University of Ceará,
Fortaleza, Ceará, Brazil
e-mail: bismarkg@dee.ufc.br

Rômulo N. de C. Almeida
Department of Electrical Engineering,
Federal University of Ceará,
Sobral, Ceará, Brazil
e-mail: rnunes@dee.ufc.br

Laurinda L. N. dos Reis[1]
Mem. IEEE
Department of Electrical Engineering,
Federal University of Ceará,
Fortaleza, Ceará, Brazil
e-mail: laurinda@dee.ufc.br

Wellington A. Silva
Department of Electrical Engineering,
Federal University of Ceará,
Fortaleza, Ceará, Brazil
e-mail: wellington@dee.ufc.br

Ricardo S. T. Pontes
Department of Electrical Engineering,
Federal University of Ceará,
Fortaleza, Ceará, Brazil
e-mail: ricthe@dee.ufc.br

Robust Control Based on Generalized Predictive Control Applied to Switched Reluctance Motor Current Loop

This paper proposes a robust control based on generalized predictive control (GPC) applied to the current control loop for a switched reluctance motor (SRM) drive. The proposed controller has two degrees of freedom where the setpoint tracking is decoupled from the load disturbance rejection at the nominal case. In addition a filter design is proposed in order to achieve good relationship among robustness, load disturbance rejection, and noise attenuation. Simulation and real experimental results are shown to illustrate the controller performance. [DOI: 10.1115/1.4026128]

1 Introduction

SRMs are an alternative and modern solution to electromechanical conversion with variable speed. The availability of high-frequency switching devices and improvements in machine design, associated with SRM intrinsic simplicity, reliability, low cost, high power capacity, and fault tolerant operation have made it a viable replacement for conventional motor drives [1,2].

SRMs have been traditionally controlled by either open loop hysteresis or closed-loop pulse-width-modulation (PWM) current controllers. Each scheme presents advantages and drawbacks with regard to parametric variations, accuracy, robustness, and dynamic response over the entire speed range. The hysteresis current controller is popular because of its inexpensive, simple, and easy-to-use architecture [3–5]. However, there are well known disadvantages, such as variable switching frequency and high ripple current, making it undesirable for many applications. On the other hand, PWM controllers provide better control loop characteristics compared to their hysteresis counterparts, although they are more complex to be designed and require more computation effort, such drawbacks can be overcome by using digital signal processors (DSPs). In addition, in order to achieve improved efficiency the SRM must operate under magnetic saturation [6]. This effect associated with the current level and the variation of magnetic reluctance with respect to rotor position results in highly nonlinear dynamics of all the machine relevant characteristics.

For the high performance operation of SRM drives, the current loop plays a major role, mainly at low speeds where the torque is only limited by the current. As a consequence, to achieve good torque control, accurate current command tracking control is required [1,2]. However if the current is not properly modulated and switched at the correct rotor position all negative effects e.g., high torque pulsation and acoustic noise are intensified. As the speed increases, the back electromotive force (EMF) increases to a level where the available voltage becomes insufficient to regulate the current, while the control system should naturally assume single pulse mode to achieve the maximum available voltage for high-speed operation. The torque can then be controlled only by properly adjusting the angles of the current pulses [6]. The ability of tracking the dynamic setpoint and recovering from load disturbances without torque ripple are two important challenges for high performance in SRM drives [7,8]. Several researchers have proposed current profiling-based methods to minimize torque ripple [1,2,9,10]. Often, proportional-integral (PI) current regulators have been applied in SRM drives with limited performance [2,11]. However, due to the aforementioned nonlinear plant characteristics, good performance, and stable operation are difficult to achieve over the entire operating range. The nonlinear characteristic of the SRM model represents a challenge to classical and advanced control techniques, thus motivating several researchers to propose current control techniques to overcome this drawback [2,11–14].

In literature, it is easy to find numerous examples about advanced control techniques in current control of SRMs using adaptive control, neural network controllers, and fuzzy logic control [15–17]. Model-based predictive control (MPC) has also been used in SRM control [18,19] aggregating a series of advantages over other methods, amongst which the following ones stand out [20,21]: (a) It is particularly attractive for users with limited knowledge about control because the concepts are very intuitive. (b) Simplicity of tuning considering both setpoint tracking and disturbance rejection. (c) A specified performance criterion is minimized on-line. (d) In the worst case, its performance is similar to a proportional-integral-derivative (PID) controller with

[1]Corresponding author.

Contributed by the Dynamic Systems Division of ASME for publication in the Journal of Dynamic Systems, Measurement, and Control. Manuscript received December 5, 2012; final manuscript received November 12, 2013; published online February 28, 2014. Assoc. Editor: YangQuan Chen.

optimal tuning. (e) Its extension to the treatment of constraints is conceptually simple, which can be systematically included during the design process. Despite of the advantages related to MPC, due to its high computational cost, real applications in drive systems are very rare and most of the papers present only simulation results [18,19,22,23]. Within this context, this paper presents a robust control structure with low computational cost based on GPC [24] which belongs to a MPC family. Although the usual argument against the GPC is its demand for processing power, this paper overcomes this issue by using a simplified version of GPC which allows obtaining a similar performance than that developed by its usual counterpart, as input constraints specifications can be included.

The paper is then organized as follows: Sec. 2 presents an overview of modeling and identification of current loop for SRM drive. A review on GPC is introduced in Sec. 3. Section 4 describes the proposed controller and its robustness and stability is analyzed in Sec. 5. In Sec. 6 presents experimental results, while the relevant conclusions are discussed in Sec. 7.

2 Modeling and Identification of SRM Drive Current Loop

Models can be derived from the physical laws governing the relationship amongst variables or empirical models derived from data obtained from the process. They can also be classified as either linear or nonlinear models. In cases where nonlinear models are used to design the control strategy, nonlinear controllers are essential to achieve improved performance. Therefore, they are not feasible in applications with fast dynamics such as SRM drives because the computational time is very limited and controllers require high computation performance. On the other hand, if linear models are used, the designed controller must be robust enough to compensate for the unmodeled dynamics. Continuous and discrete linear models for SRMs are described as follows.

2.1 Small Signal Modeling of SRM Drives. An asymmetrical bridge converter applied to SRM drives can be modeled using the small-signal technique relating the duty cycle to the output current. Considering the average voltage across the phase winding during one switching period, the transfer function is given by [25,26]

$$G(s) = \left(\frac{2V_{dc}}{\omega_r \kappa + R_a}\right) \frac{1}{\left(\frac{L_j}{\omega_r \kappa + R_a}\right)s + 1} \tag{1}$$

where ω_r is the speed, κ is the gradient of the inductance varying with the rotor position θ_r, L_j is the inductance over one switching period, and R_a is the phase resistance. Since L_j and κ vary with i_j and θ_r, the transfer function from the duty cycle to the output current contains a single moving pole and variable static gain, according to Eq. (1). The pulse-width modulator is supposed to generate duty cycle D, which is proportional to the compensator output voltage. In order to determine the uncertain set based on variations of the system parameters, a multiplicative uncertainty model is proposed as

$$G(s) = G_n(s)(1 + \delta G(s)) \tag{2}$$

where $G_n(s)$ is nominal plant, $\delta G(s)$ is the multiplicative uncertainty. The upper bound of $|\delta G(j\omega)|$ is given by

$$\overline{\delta G}(\omega) = \max\left|\frac{G(j\omega) - G_n(j\omega)}{G_n(j\omega)}\right|, \forall\omega \tag{3}$$

The uncertainties are given by variations on L_j and κ, within the range $[L_{\min}(\theta_r); L_{\max}(\theta_r)]$ and $[\kappa_{\min}(\theta_r); \kappa_{\max}(\theta_r)]$, respectively.

2.2 Discrete Model Identification and Simplification. The model transfer function given in Eq. (1) can be represented in a general form as

$$G_n(s) = \frac{K_g}{\tau s + 1} \tag{4}$$

where K_g is the gain of the plant and τ is the time constant.

The procedure to determine K_g and τ is not simple when no information is provided by the manufacturer or even the machine dimensions are unknown. One way to determine such parameters is through the machine experimentation or complex computational simulations. Another alternative is to estimate them using system identification without disturbing the regular machine operation. A practical identification based on setpoint relay was implemented in Ref. [26]. A three-phase SRM was used, whose characteristics are: 12/8, 80 V_{dc}, 3.5 A, series resistance $r_s = 2.4\Omega$, rotor speed at 400 rpm. The inductance varies from a minimum value $L_u = 8$ mH to a maximum one $L_a = 52$ mH, what occurs at every 45 mechanical degrees. The algorithm is simple and requires small tuning times [14]. As a result of this identification procedure, the transfer function of SRM loop current is given by

$$G(z) = \frac{0.03259z^{-1}}{1 - 0.9996z^{-1}} \tag{5}$$

By analyzing the discrete transfer function given in Eq. (5), it can be observed that the model pole is close enough to the unity, as the result can be approximated by a discrete integrator

$$G(z) = \frac{0.03259z^{-1}}{1 - z^{-1}} \tag{6}$$

This approximation allows simplifying the controller design when intended for embedded systems.

3 GPC Approach to Model Predictive Control

The GPC algorithm consists in applying a control sequence that minimizes the multistage cost function in the form [24]

$$J = \sum_{j=N_1}^{N_2} [y(t+j|t) - w(t+j)]^2 + \sum_{j=0}^{N_u - 1} \lambda[\Delta u(t+j|t)]^2 \tag{7}$$

where N_1 and N_2 are the minimum and maximum costing horizons, respectively, N_u is the control horizon, λ is the control weight, $w(t+j)$ is a future setpoint or reference sequence, $\Delta u(t)$ is the incremental control action ($\Delta = 1 - q^{-1}$; as q^{-1} represents the backward shift operator) and $y(t+j|t)$ is the optimum j-step ahead prediction of the system output $y(t)$ on data up to time t.

The solution of this optimization problem is a crucial step in MPC algorithms. The numerical complexity depends on the characteristics of the models in terms of linearity, constraints, number of manipulated and controlled variables among other factors. For linear models without constraints, the MPC optimization can be performed analytically [27].

3.1 Computing the Predictions. The process dynamics can be represented using the controlled auto-regressive and integrated moving average model [24]

$$A(q^{-1})y(t) = B(q^{-1})u(t) + \frac{C(q^{-1})}{\Delta}e(t) \tag{8}$$

where $e(t)$ is uncorrelated (white) noise with zero mean value, $A(q^{-1})$, $B(q^{-1})$, and $C(q^{-1})$ are polynomials in the backward shift operator q^{-1} in the form

$$A(q^{-1}) = 1 + a_1 q^{-1} + a_2 q^{-2} + \ldots + a_{na} q^{-na} \quad (9)$$

$$B(q^{-1}) = b_0 + b_1 q^{-1} + b_2 q^{-2} + \ldots + b_{nb} q^{-nb} \quad (10)$$

$$C(q^{-1}) = 1 + c_1 q^{-1} + c_2 q^{-2} + \ldots + c_{nc} q^{-nc} \quad (11)$$

The future outputs can be computed by using filtering techniques or Diophantine equations [27] while this work uses the second approach. To compute the future outputs $y(t+j)$ for $j = N_1, \ldots, N_2$, the following Diophantine equation must be solved:

$$C(q^{-1}) = E_j(q^{-1})\Delta A(q^{-1}) + q^{-j} F_j(q^{-1}) \quad (12)$$

where $E_j(q^{-1})$ and $F_j(q^{-1})$ are uniquely defined polynomials with degrees $j-1$ and na, respectively.

Using Eqs. (8) and (12) the future process output can be described by

$$y(t+j) = \frac{F_j(q^{-1})}{C(q^{-1})} y(t) + \frac{E_j(q^{-1}) B(q^{-1})}{C(q^{-1})} \Delta u(t+j-1) + E_j(q^{-1}) e(t+j) \quad (13)$$

As the degree of $E_j(q^{-1})$ is $j-1$, then all the noise terms are in the future, and therefore the optimal prediction can be obtained replacing $e(t+j)$ by its expected value (zero) as

$$y(t+j|t) = \frac{F_j(q^{-1})}{C(q^{-1})} y(t) + \frac{E_j(q^{-1}) B(q^{-1})}{C(q^{-1})} \Delta u(t+j-1|t) \quad (14)$$

From above equation, the past control inputs can be separated solving a new Diophantine equation

$$E_j(q^{-1}) B(q^{-1}) = H_j(q^{-1}) C(q^{-1}) + q^{-j} I_j(q^{-1}) \quad (15)$$

where $H_j(q^{-1})$ has degree $j-1$ and $I_j(q^{-1})$ has degree $ni = \max(na, nb-j-1)$. By using Eqs. (14) and (15), the prediction output can be written as

$$y(t+j|t) = \frac{F_j(q^{-1})}{C(q^{-1})} y(t) + \frac{I_j(q^{-1})}{C(q^{-1})} \Delta u(t-1) + H_j(q^{-1}) \Delta u(t+j-1|t) \quad (16)$$

which can be expressed in a vector form as

$$\mathbf{y} = \mathbf{F}(q^{-1}) \frac{y(t)}{C(q^{-1})} + \mathbf{I}(q^{-1}) \frac{\Delta u(t-1)}{C(q^{-1})} + \mathbf{G}\Delta\mathbf{u} \quad (17)$$

where $\mathbf{y} = [y(t+N_1|t)\ y(t+N_1+1|t) \ldots y(t+N_2|t)]^T$, $\Delta\mathbf{u} = [\Delta u(t|t) u(t+1|t) \ldots u(t+N_u-1|t)]^T$, $\mathbf{G}$ is a $N \times N_u$ constant matrix based on the coefficients of $H_j(q^{-1})$, while $\mathbf{F}(q^{-1})$ and $\mathbf{I}(q^{-1})$ are polynomial vectors.

3.2 Optimization Procedure. From controller implementation standpoint, an analytical solution with low computational cost is important. Thus, this work is concerned with the investigation of a special case where $N_u = 1$, $N_1 = 1$, $N_2 = N$, and $\lambda = 0$, which represents the best tradeoff between the computational cost and close-loop performance [28]. Then, the optimal input is Ref. [29]

$$\Delta u(t) = (\mathbf{G}^T\mathbf{G})^{-1}\mathbf{G}^T(\mathbf{w} - \mathbf{f}) = \mathbf{k}(\mathbf{w} - \mathbf{f}) \quad (18)$$

where $\mathbf{k}$ is a constant vector with dimension $1 \times N$, $\mathbf{w}$ is a vector which contains the future reference and $\mathbf{f} = \mathbf{F}(q^{-1})(y(t)/C(q^{-1})) + \mathbf{I}(q^{-1})(\Delta u(t-1)/C(q^{-1}))$ (or free response).

Through some manipulations, Eq. (18) can be written in the RST form

$$u(t) = \frac{1}{\Delta R(q^{-1})} \left(T(q^{-1}) r(t) - S(q^{-1}) y(t) \right) \quad (19)$$

where $r(t) = w(t+j)$ is the setpoint, $T(q^{-1}) = C(q^{-1}) \sum_{i=1}^{N} \mathbf{k}(i)$, $S(q^{-1}) = \sum_{i=1}^{N} \mathbf{k}(i) F_i(q^{-1})$, and $R(q^{-1}) = C(q^{-1}) + q^{-1} \sum_{i=1}^{N} \mathbf{k}(i) I_i(q^{-1})$. The RST structure is important from control analysis standpoint because it can be derived properties such as stability and robustness. This paper does not cover the constraint case of MPC. Nevertheless, the real plant has input saturation constraints within the range from 0% to 100%. Thus, if the maximum or minimum plant input limitations are achieved, a hard limitation at the control input is applied resulting in a suboptimal solution, also known as clipping. This solution does not need any additional antiwindup technique in case of $N_u = 1$ [29].

4 Robust GPCBC Applied to SRM Current Loop

The model which relates the duty cycle to the SRM current loop is given by

$$(1 - q^{-1}) y(t) = b_0 u(t-1) + \frac{C(q^{-1})}{\Delta} e(t) \quad (20)$$

where b_0 is a constant related to the velocity gain of the plant and $C(q^{-1})$ is a monic polynomial that can be treated as a filter [27]. The selection of $C(q^{-1})$ is not a trivial matter, while some guidelines for open-loop stable processes and some case studies can be found in literature [30].

In this study, the process is of first-order and has integrative nature. It is then enough to use a filter with degree $nc = 2$ in order to attenuate the noise, considering that it is properly tuned [27]. Thus, the proposed filter is given by

$$C(q^{-1}) = 1 + c_1 q^{-1} + c_2 q^{-2} \quad (21)$$

where c_1 and c_2 are constants which must be tuned considering noise attenuation, disturbance rejection, and robustness.

Considering Eqs. (20) and (21), the control input $u(t)$ in Eq. (19) can be calculated explicitly by performing some mathematical manipulation. Thus, the control polynomials R, S, and T are given by

$$T(q^{-1}) = \frac{(1-\alpha) C(q^{-1})}{b_0} \quad (22)$$

$$R(q^{-1}) = 1 - \alpha c_2 q^{-1} \quad (23)$$

$$S(q^{-1}) = \frac{2 - \alpha + c_1 + \alpha c_2 - (1 + \alpha c_1 + (2\alpha - 1) c_2) q^{-1}}{b_0} \quad (24)$$

$$\alpha = 1 - \frac{1 + 2 + 3 + \ldots + N}{1 + 2^2 + 3^2 + \ldots + N^2} \quad (25)$$

It is important to notice that polynomials R, S, and T contain the parameter α, which on the other hand depends on N. From Eq. (25), it can be seen that α varies from 0 to 1 when the prediction horizon N varies from 1 to ∞. If N is used as a tuning parameter, then α will have discrete values thus making precise tuning impossible. To overcome this problem, the use of α as a direct tuning parameter is proposed.

4.1 Nominal Input-Output Transfer Functions. The block diagram of the proposed Robust GPC-based control (GPCBC) can be represented in the classical RST structure as illustrated in Fig. 1. To understand the nominal behavior, the transfer functions relating the reference to the output, the input disturbance to the

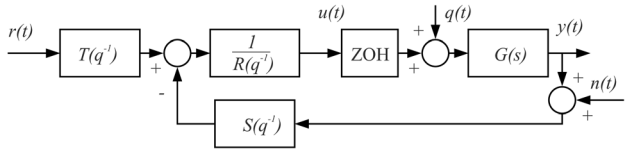

Fig. 1 Classical RST structure

Table 1 Proposed filters

Filter name	β/σ
C_0	tan(0 deg)
C_{30}	tan(30 deg)
C_{45}	tan(45 deg)
C_{65}	tan(60 deg)
C_{75}	tan(75 deg)

output, the noise to the control input and the noise to the output are calculated as follows:

$$H_{yr}(z) = \mathcal{Z}\left\{\frac{y(t)}{r(t)}\right\} = \frac{1-\alpha}{z-\alpha}, \tag{26}$$

$$H_{yq}(z) = \mathcal{Z}\left\{\frac{y(t)}{q(t)}\right\} = \frac{z^{-1}b_0R(z)\Delta(z)}{C(z)(1-\alpha z^{-1})} \tag{27}$$

$$H_{un}(z) = \mathcal{Z}\left\{\frac{u(t)}{n(t)}\right\} = \frac{-S(z)\Delta(z)}{C(z)(1-\alpha z^{-1})} \tag{28}$$

$$H_{yn}(z) = \mathcal{Z}\left\{\frac{y(t)}{n(t)}\right\} = \frac{-z^{-1}b_0S(z)}{C(z)(1-\alpha z^{-1})} \tag{29}$$

where $\mathcal{Z}\{.\}$ denotes z-transform, $q(t)$ is an input disturbance, and $n(t)$ is a measurement noise signal at a given discrete instant t.

Equation (26) shows that $H_{yr}(z)$ is a first-order transfer function which only depends just on α. Therefore faster or slower setpoint responses can be achieved by decreasing or increasing α, respectively. On the other hand, $C(z)$ can be used to modify the disturbance rejection response Eq. (27) while acting as a measurement noise filter in order to attenuate noise effect in both control and output signals, Eqs. (28) and (29), respectively.

4.2 Filter Design for Disturbance Rejection and Noise Attenuation. Equations (27) and (28) evidence that both disturbance rejection and noise attenuation depend on $C(q^{-1})$, as the tuning of the related parameters is crucial. This work assumes that $C(q^{-1})$ has roots with identical real part, while Eq. (21) can be rewritten as

$$C(q^{-1}) = (1-e^{-\sigma+i\beta}q^{-1})(1-e^{-\sigma-i\beta}q^{-1}) \tag{30}$$

where σ and β are tuning parameters, and i is the imaginary operator.

The ratio β/σ imposes certain characteristics to the filter C, and therefore a set of filters with different ratios β/σ can be defined according to Table 1.

To show the influence of each filter $C = C_m$, $m = 0, 30, ..., 75$, on disturbance and noise rejection, several simulations were performed according with the following criteria:

(a) First, a set of different values for σ is defined within in a desired range ($\sigma = \sigma_k, k = 1, ..., n_k$) while β was calculated ($\beta = \beta_k, k = 1, ..., n_k$) for each value of σ keeping the ratio β/σ constant as defined in Table 1.
(b) Then, for each filter C_m, with $\sigma = \sigma_k$ and $\beta = \beta_k$, the respective controller was properly designed, corresponding to polynomials R, S, and T.

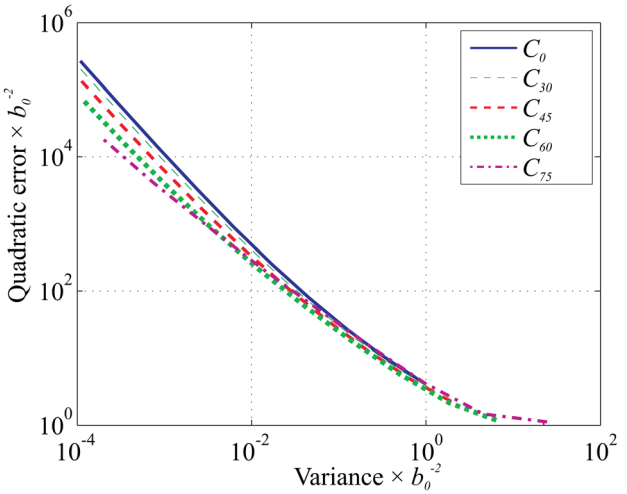

Fig. 2 Relationship between quadratic error and variance for each studied filter

Table 2 Variance of the filters

Quadratic error $E_q = 10^4 \times b_0^2$		
Filter	σ	$V_u \times 10^{-4} \times b_0^{-2}$
C_0	0.031	10.6
C_{30}	0.028	8.9
C_{45}	0.025	7.0
C_{65}	0.019	4.9
C_{75}	0.012	3.4

(c) From the aforementioned controllers, the quadratic error E_q and the control input variance V_u were obtained considering a unit step disturbance $q(t)$ ($r(t) = 0$, $n(t) = 0$) and zero-mean noise $n(t)$ with unity variance ($r(t) = 0$ and $q(t) = 0$), respectively.

The simulated curves that relate E_q and V_u for the set of studied filters are shown in Fig. 2. The best relationships between E_q and V_u are given by the lower curves. For instance, if σ is tuned to obtain $E_q = 10^4 \times b_0^2$ then the variance will vary between the controllers as shown in Table 2. It can be seen that the variance changes more than 300% from the best case to the worst one. If disturbance rejection and noise attenuation are the sole criteria to design the filter C, then the best option is to use the filter $C = C_{75}$. Besides, robustness must be also taken into account in order to obtain a final decision.

5 Robustness and Stability Analysis

The robustness analysis is performed considering that the modeling errors of the SRM drive can be represented as unstructured uncertainties, i.e.,: $G(z) = G_n(z) + \Delta G(z) = G_n(z)(1 + \delta G(z))$ while G_n is the nominal plant. Besides, let us consider that an upper bound for the norm of $\delta G(e^{i\Omega})$ is given by $\overline{\delta G}(\Omega)$ for $0 \le \Omega < \pi$ [31].

In order to maintain robust closed-loop stability, the following statement must be satisfied [32]:

$$\overline{\delta G}(\Omega) \le I_r(\Omega) = \frac{|C(e^{-i\Omega})(1-\alpha e^{-i\Omega})|}{|S(e^{-i\Omega})b_0e^{-i\Omega}|} \tag{31}$$

where $\Omega \in [0, \pi]$, and $I_r(\Omega)$ is defined as the robustness index of the controller. It can be observed that $I_r(\Omega)$ depends on α and $C(e^{-i\Omega})$, where $C(e^{-i\Omega})$ is a tuning factor for robustness.

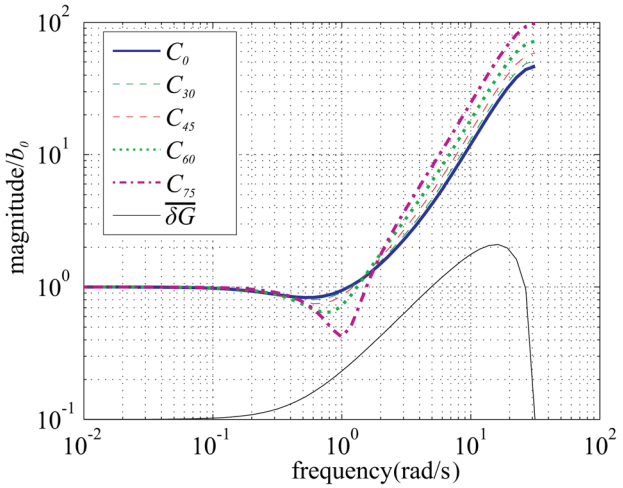

Fig. 3 Robustness index

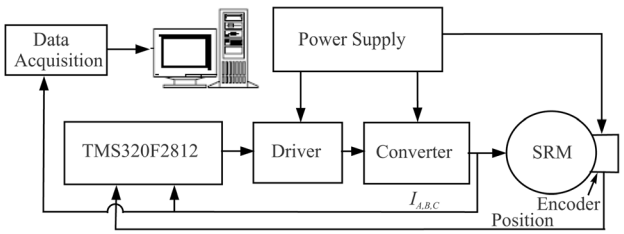

Fig. 4 The experimental setup of the SRM drive

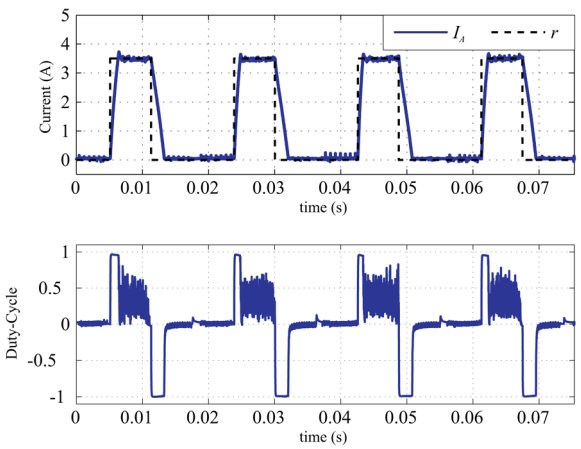

Fig. 5 Experimental current and duty-cycle through SRM winding A using GPCBC controller

Figure 3 illustrates the robustness index I_r of the proposed controllers and the upper bound of the multiplicative error $\overline{\delta G}$, which considers ± 10% uncertainties on velocity gain (b_0) and two samples for time delay. At low frequencies, it is observed that the robustness index of all controllers is the same; at mid-frequencies, the controllers with larger β/σ ratios are less robust, specially C_{75} which is fair less robust than the remaining filters; at high frequencies, all the controllers have high robustness, particularly those with larger β/σ ratio. Considering a general robustness analysis at mid-frequencies, where robustness is supposed to be important [20], the controllers with smaller β/σ ratio are more robust, although the difference from C_{45} to C_0 is negligible.

For a general analysis, the results from Sec. 4.2 are considered. Besides, it has been shown that the best controller for disturbance rejection and noise attenuation is the one with the largest β/σ ratio. One must notice that σ is the only free tuning parameter of $C(q^{-1})$. It can be tuned with lower values to obtain better noise attenuation and robustness at the cost of worse disturbance rejection, or with higher values to obtain better disturbance rejection at the cost of worse noise attenuation and robustness. Thus, by using the robustness analysis, the controller C_{45} can be considered as the best choice [27].

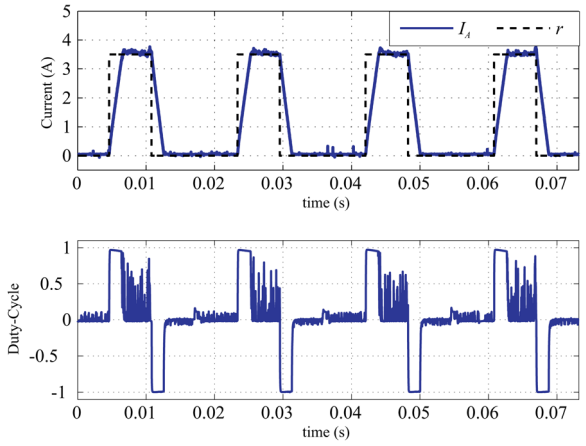

Fig. 6 Experimental current and duty-cycle through SRM winding A using SGPC controller

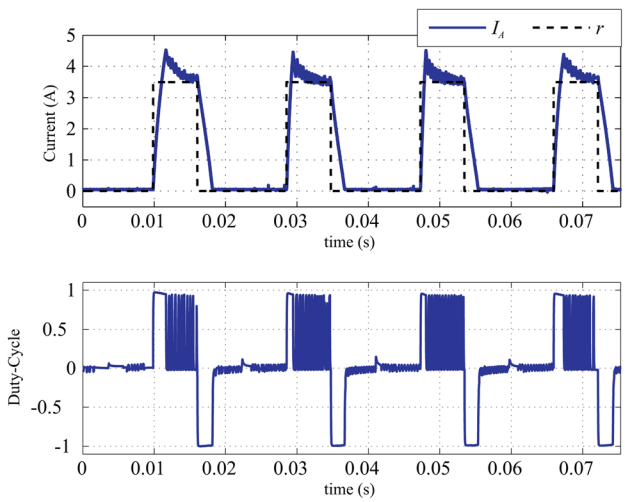

Fig. 7 Experimental current and duty-cycle through SRM winding A using PI controller with step load

6 Experimental Results

To explore the effectiveness of proposed controller, experimental tests have been carried out. The proposed controller GPCBC was compared with both a simplified GPC (SGPC) and a conventional PID controller. The controllers have been implemented in a prototype using a digital signal processor TMS320F2812 (DSP), and a classical asymmetric bridge converter, with switching frequency of 25 kHz. The experimental setup is presented in Fig. 4.

The plant model used by the controllers is described by Eq. (5). The proposed controller (GPCBC) parameters were chosen as $\alpha = 0.5$ in order to obtain a desired time constant to setpoint tracking of approximately 60 μs. The filter was adjusted with $\sigma = 0.3$ ($C_{45}(q^{-1}) = 1 - 1.42q^{-1} + 0.55q^{-2}$) to achieve the desired trade-off among robustness, noise attenuation, and disturbance rejection. In the SGPC case, $C = 1$ and α becomes the only tuning parameter, it is worth to mention that α is set at 0.8 in order to

Table 3 Performance index

Index	GPCBC	SGPC	PI
Quadratic error (E_q)	0.0022	0.0047	0.1148
Average overshoot (%)	0.0491	0.0680	0.2762
Input variance (V_u)	0.0376	0.0402	0.1636

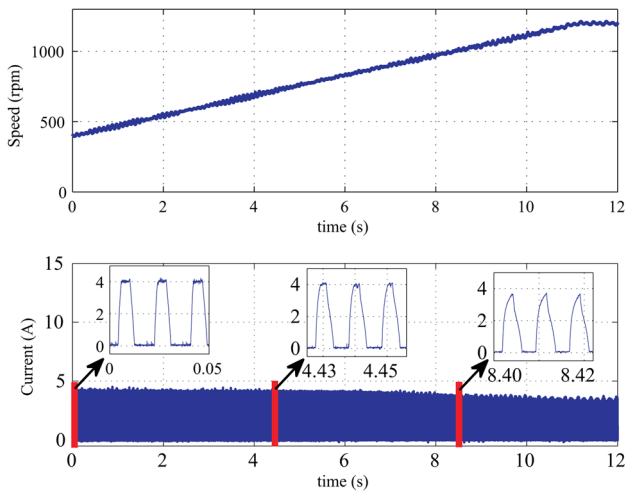

Fig. 8 Experimental speed and current through SRM winding A using GPCBC controller, 400–1200 rpm

achieve robustness similar to GPCBC. The PI controller was adjusted in order to achieve time constant to setpoint tracking similar to GPCBC, where the relevant parameters are $K_p = 230.67$ and $T_i = 1.98 \times 10^3$ [33].

In order to illustrate the results to setpoint tracking of GPCBC, SGPC and PI experimental tests were performed at 400 rpm, while the results are shown in Figs. 5–7. The waveforms represent the reference signal ($r = 3.5$ *A*), the phase current through winding *A* (I_A), and the variation of the duty-cycle (control input) for the SRM drive at nominal speed.

It can be observed that all controllers are able to track the predetermined reference. Aiming to perform a quantitative analysis, the input variance V_u, the quadratic error E_q, and the average percent overshoot are the adopted parameters. The values for V_u and E_q are computed as

$$V_u = \frac{1}{M}\sum_{k=1}^{M}(u(k) - \bar{u})^2 \tag{32}$$

$$E_q = \frac{1}{M}\sum_{k=1}^{M}(e(k))^2 \tag{33}$$

where $\bar{u}$ is average input and M is the number of samples. The results are shown in Table 3.

According to Figs. 5–7 and Table 3, the quadratic error of the proposed controller (GPCBC) is about half of that for SGPC. Besides, it corresponds to about one fifth of the error obtained with the PI controller. The average percent overshoot for the GPCBC and SGPC are 5% and 7%, respectively, while the value obtained with the PI controller is about 27%. Moreover, the stochastic performance of control input of the proposed controller is 3.7%, being 4% and 16% for SGPC and the PI controller, respectively, thus representing an important improvement from the control standpoint. It is important to mention that the sequential switching logic of the converter disconnects the phase winding, which is submitted to a negative voltage. It causes the phase current flowing through the freewheeling diodes to be null. At this

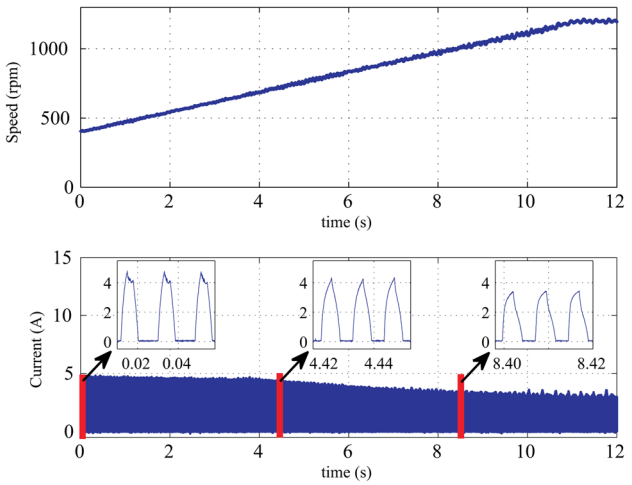

Fig. 9 Experimental speed and current through SRM winding A using PI controller, 400–1200 rpm

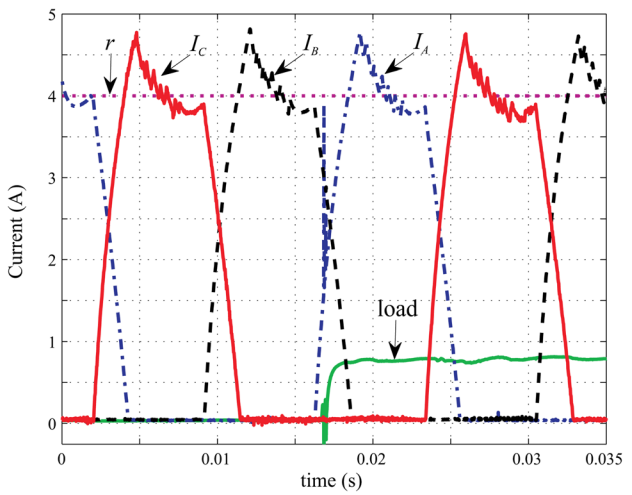

Fig. 10 Experimental currents through SRM windings and load using PI controller, at 350 rpm

point the controller acts to control the next active phase. It must be also noticed that the input control signal is constrained within the range from 0% to 100% as shown in Figs. 5–7.

In order to show the performance of GPCBC and PI controllers over a wide range operation, the motor speed varies in the ramp shape from 400 to 1200 rpm as illustrated in Figs. 8 and 9.

It can be seen that at high speeds the current control is performed by varying the dwell angle and the controller falls into single pulse mode, as presented in Ref. [6]. Besides, it can be stated that GPCBC maintains the desired current response characteristics at medium and low speeds, while the PI controller presents a response degradation as the speed operation point changes.

To evaluate the robustness of GPCBC and PI controllers to disturbances a mechanical load step was applied by using a pure resistive load rated at around 12 W, which is connected to the generator attached to the SRM operating with constant torque at 350 rpm [6]. The results are illustrated in Figs. 10 and 11. It can be seen that the GPCBC response is almost unaffected by the load disturbance while the PI controller is clearly affected.

All the aforementioned validation tests confirm that the proposed controller is suitable for the operation at low, medium, and high speed and is able to reject load disturbances in a SRM drive system.

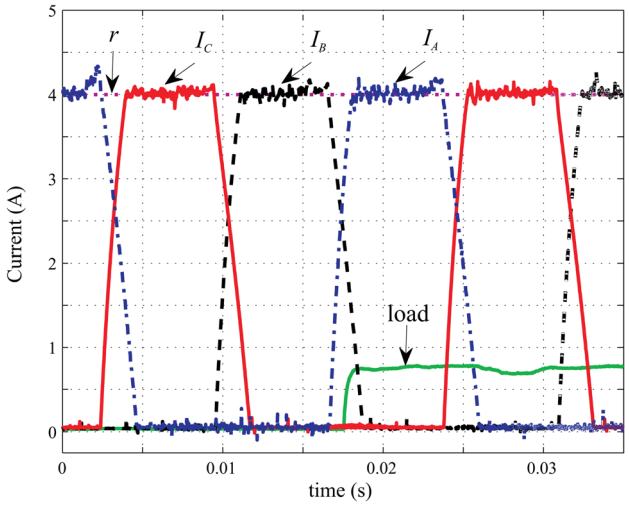

Fig. 11 Experimental currents through SRM windings and load using GPCBC controller, at 350 rpm

7 Conclusion

A robust control based on model predictive control has been successfully applied to the current control loop of a SRM drive. The approach has proven to be suitable for SRM drive applications in terms of the achievable control performance, robustness against model mismatches, and unexpected dynamic behavior, as well as in terms of low online computation burden, being suitable for practical use in a wide variety of embedded systems. The tuning procedure of the proposed controller is intuitive and the set-point tracking is decoupled from the disturbance rejection. A filter design has been proposed in order to obtain a good relationship among robustness, load disturbance rejection, and noise attenuation. Even though no specific experiments regarding noise rejection have been carried out, it can be observed that the regular noise inherent to the SRM drive system does not affect neither the system stability nor its operation significantly, as predicted in the simulations results. Experimental results have also demonstrated the feasibility of the proposed SRM drive control scheme.

References

[1] Schroder, G., and Bekiesch, J., 2005, "Current Control for the Switched Reluctance Motor With Enhanced Performance," European Conference on Power Electronics and Applications—PESC, pp. P.1–P.8.

[2] Lin, Z., Reay, D. S., Williams, B. W., and He, X., 2004, "High Performance Current Control for Switched Reluctance Motors With On-Line Modeling," IEEE Power Electronics Specialists Conference—PESC, Vol. 2, pp. 1246–1251.

[3] Amato, D., Tonielle, A., and Tilli, A., 2001, "An Improved Sequential Hysteresis Current Controller for Three-Phase Inverter: Design and Hardware Implementation," IEEE International Conference on Proceedings of the Control Applications—CCA, pp. 294–300.

[4] Bianco, C. G. L., Tonielli, A., and Filicori, F., 1996, "A Prototype Controller for Variable Reluctance Motors," IEEE Trans. Ind. Electron., **43**, pp. 207–216.

[5] Benhadria, M., Kendouci, K., and Mazari, B., 2006, "Torque Ripple Minimization of Switched Reluctance Motor Using Hysteresis Current Control," IEEE International Symposium on Industrial Electronics, Vol. 3, pp. 2158–2162.

[6] Miller, T. J. E., 2001, *Electronic Control of Switched Reluctance Machines*, Newnes, Oxford, UK.

[7] Inderka, R. B., Menne, M., and De Doncker, R. W. A. A., 2002, "Control of Switched Reluctance Drives for Electric Vehicle Applications," IEEE Trans. Ind. Electron., **49**, pp. 48–53.

[8] Husain, I., and Hossain, S. A., 2005, "Modeling, Simulation, and Control of Switched Reluctance Motor Drives," IEEE Trans. Ind. Electron., **52**, pp. 1625–1634.

[9] Sahoo, S. K., Panda, S. K., and Xu, J. X., 2004, "Iterative Learning-Based High-Performance Current Controller for Switched Reluctance Motors," IEEE Trans. Energy Convers., **19**, pp. 491–498.

[10] Xue, X. D., Cheng, K. W. E., and Ho, S. L., 2009, "Optimization and Evaluation of Torque-Sharing Functions for Torque Ripple Minimization in Switched Reluctance Motor Drives," IEEE Trans. Power Electron., **24**(9), pp. 2076–2090.

[11] Liu, C.-Y., Hou, X.-C., Cui, Y.-L., and Liu, J.-M., 2003, "Research for Speed Controller of Switched Reluctance Motor Using F-PID Control," International Conference on Machine Learning and Cybernetics, Vol. 4, pp. 2530–2533.

[12] Russa, K., Husain, I., andElbuluk, M. E., 2000, "A Self-Tuning Controller for Switched Reluctance Motors," IEEE Trans. Power Electron., **15**(3), pp. 545–552.

[13] Yang, Y., and Zhang, Y., 2005, "Sliding Mode-PI Control of Switched Reluctance Motor Drives for EV," Proceedings of the Eighth International Conference on Electrical Machines and Systems—ICEMS, Vol. 1, pp. 603–607.

[14] Luo, R., Qin, S. J., and Chen, D., 1998, "A New Approach to Closed Loop Autotuning for PID Controllers," Proceedings of the American Control Conference, pp. 348–352.

[15] Mitsukura, Y., Yamamoto, T., Kaneda, M., Fukumi, M., Akamatsu, N., and Shah, S. L., 2000, "Design and Experimental Evaluation of Self-Tuning PID Controller Using Evolutionary Computation," Proceedings IFAC Workshop on Digital Control: Past, Present and Future of PID Control, pp. 553–558.

[16] Vejian Rajandran, R., Ramasamy, G., and Sahoo, N., 2005, "Flux Linkage Model Optimization Using Binary Coded Genetic Algorithm for Switched Reluctance Motor," International Conference on Power Electronics and Drives Systems—PEDS, Vol. 2, pp. 898–902.

[17] Mirzaeian-Dehkordi, B., and Moallem, P., 2006, "Genetic Algorithm Based Optimal Design of Switching Circuit Parameters for a Switched Reluctance Motor Drive," International Conference on Power Electronics, Drives, and Energy Systems—PEDES, pp. 1–6.

[18] Sadeghzadeh, A., and Araabi, B. N., 2006, "Auto-Tune Predictive Control of Switched Reluctance Motor," IEEE International Symposium on Industrial Electronics, Vol. 1, pp. 335–340.

[19] Peyrl, H., Papafotiou, G., and Morari, M., 2009, "Model Predictive Torque Control of a Switched Reluctance Motor," IEEE International Conference on Industrial Technology—ICIT, pp. 1–6.

[20] Thomsen, S., Hoffmann, N., and Fuchs, F. W., 2011, "PI Control, PI-Based State Space Control, and Model-Based Predictive Control for Drive Systems With Elastically Coupled Loads a Comparative Study," IEEE Trans. Power Electron., **58**(8), pp. 3647–3656.

[21] Kennel, R., Linder, A., and Linke, M., 2001, "Generalized Predictive Control (GPC)-Ready for Use in Drive Applications?," IEEE 32nd Annual Power Electronics Specialists Conference—PESC, pp. 1839–1844.

[22] Mayne, D. Q., Rawlings, J. B., Rao, C. V., andScokaert, P. O. M., 2000, "Constrained Model Predictive Control: Stability and Optimality," Automatica, **36**(6), pp. 789–814.

[23] Li, H., and Shi, Y., 2013, "Output Feedback Predictive Control for Constrained Linear Systems With Intermittent Measurements," Syst. Control Lett., **62**(4), pp. 345–354.

[24] Clarke, D. W., Mothadi, C., and Tuffs, P. S., 1987, "Generalized Predictive Control. Part I the Basic Algorithm and Part II Extensions and Interpretations," Automatica, **23**(2), pp. 137–160.

[25] Zhu, G., Wei, H., Kornetzky, P., and Batarseh, I., 1999, "Small-Signal Modeling of a Single-Switch AC/DC Power-Factor-Correction Circuit," IEEE Trans. Power Electron., **14**(6), pp. 1142–1148.

[26] dos Reis, L. L. N., Coelho, A. A. R., Almeida, O. M., and Campos, J. C. T., 2009, "Modeling and Controller Performance Assessment for a Switched Reluctance Motor Drive Based on Setpoint Relay," ISA Trans., **48**(2), pp. 1142–1148.

[27] Camacho, E. F., and Bordons, C., 2004, *Model Predictive Control*, Springer-Verlag, London.

[28] Torrico, B. C., Roca, L., Normey-Rico, J. E., Guzman, J. L., and Yebra, L., 2010, "Robust Nonlinear Predictive Control Applied to a Solar Collector Field in a Solar Desalination Plant," IEEE Trans. Control Syst. Technol., **18**(6), pp. 1430–1439.

[29] De Keyser, R., 2003, "Model Based Predictive Control," *Invited Chapter in UNESCO Encyclopedia of Life Support Systems (EoLSS)*, p. 30.

[30] Yoon, T. W., and Clarke, D. W., 1994, *Advances in Model-Based Predictive Control, Towards Robust Adaptive Predictive Control*, Oxford University Press, Oxford, UK, pp. 402–414.

[31] Morari, M., and Zafiriou, E., 1989, *Robust Process Control*, Prentice Hall, Englewood Cliffs, NJ.

[32] Skogestad, S., and Postlethwaite, I., 1996, *Multivariable Feedback Control: Analysis and Design*, Wiley, Chichester, UK.

[33] Åström, K. J., and Hägglund, T., 2006, *Advanced PID Control*, ISA—Instrumentation, Systems and Automation Society, Research Triangle Park, NC.